Extended π-conjugated pyrene derivatives: structural, photophysical and electrochemical properties

Xing Feng,*[†,‡] Nobuyuki Seto,[†] Chuan-Zeng Wang, [†] Taisuke Matsumoto,[§] Junji Tanaka,[§] Mark R. J. Elsegood,[‖] Lynne Horsburgh,[‖] Carl Redshaw[⊥] and Takehiko Yamato*[†]

[†]Department of Applied Chemistry, Faculty of Science and Engineering, Saga University, Honjo-machi 1, Saga 840-8502 Japan

[‡]Beijing Institute of Graphic Communication, Beijing, 102600, P. R. China

[§]Institute of Materials Chemistry and Engineering, Kyushu University, 6-1, Kasugakoen, Kasuga 816-8580, Japan

[‖]Chemistry Department, Loughborough University, Loughborough, Leicestershire LE11 3TU, UK

[⊥]Department of Chemistry, The University of Hull, Cottingham Road, Hull, Yorkshire HU6 7RX, UK

E-mail: yamatot@cc.saga-u.ac.jp, hyxhn@sina.com

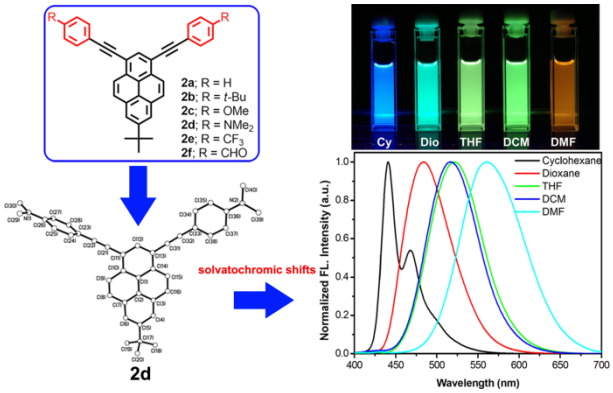

ABSTRACT: This article presents a set of extended π-conjugated pyrene derivatives, namely 1,3-di(arylethynyl)-7-*tert*-butylpyrene, which were synthesized by a Pd-catalyzed Sonogashira coupling reaction of 1,3-dibromo-7-*tert*-butylpyrene with the corresponding arylethynyl group in good yield. Despite the presence of the *tert*-butyl group located at the 7-position of pyrene, X-ray crystallographic analyses show that the planarity of the *Y*-shaped molecules still exhibits strong face-to-face π-π

stacking in the solid state; all of the compounds exhibit blue or green emission with high quantum yields (QYs) in dichloromethane. DFT calculations and electrochemistry revealed that this category of compound possesses hole-transporting characteristics. In addition, with strong electron-donating ($–N(CH_3)_2$) or electron-withdrawing (–CHO) groups in **2d** or **2f**, these molecules displayed efficient intramolecular charge-transfer (ICT) emissions with solvatochromic shifts from blue to yellow (green) on increasing the solvent polarity. Furthermore, the compounds possess strong CT characteristics but displayed relatively low QYs.

1. Introduction

Large π-conjugated organic materials have attracted increasing attention in recent years, due to facile band-gap and colour control by structural modification, which makes them suitable for potential application in high performance organic electronics,[1] such as organic light emitting diodes (OLEDs),[2] liquid-crystal displays,[3] organic field effect transistors (OFETs)[4,5] and organic photovoltaic cells (OPVs),[6] as well as optical storage devices.[7] Extension of the π-conjugation chromophores contributes to a lowering of the HOMO-LUMO gap, leading to a red-shift in absorption and emission spectra with increasing fluorescence quantum yields. In addition, molecules which possess π-conjugation with a planar structure would enhance charge carrier transport in optoelectronic applications by self-assembly *via* intermolecular π-π stacking.[8]

Pyrene[9] is made up of four fused aromatic rings with a large π-electron system, which exhibits good solution-processable properties with an excellent blue emission spectrum (with a long excited-state lifetime, high fluorescence intensity and quantum yield). However, the deployment of pyrene as a host material in blue light-emitting diodes is scarce, due to its tendency to readily aggregate in most media. Several research groups including ours have reported many new types of pyrene derivatives, and various substituent groups have been attached to the pyrene core by –C–C–, –C–N– or –C≡C– bonds for suppressing excitation emission.[10-15] Some ethynyl-substituted pyrene-based compounds displayed more intriguing fluorescence

characteristics, for instance, Ziessel *et al* reported a greenish luminescent 1,3,6,8-tetra-(4-ethynylphenylaminoacyl) pyrene with stable liquid crystalline properties for the fabrication of OLED-like devices;[16] Kim and coworkers synthesized a series of 1,3,6,8-tetrakis(ethynyl)-pyrenes functionalized with varying numbers of *N*,*N*-dimethyaniline and 1-(trifluoromethyl)-benzene moieties as peripheral electron-donors and acceptors for chemiluminescent (ECL) active materials, that exhibited enhanced charge transfer compared with 1,3,6,8-tetra-*N*,*N*-dimethyaniline (or 1,3,6,8-tetra-trifluoromethyl-benzene).[17,18] Interestingly, Adachi *et al* have designed a number of inverted singlet-triplet (iST) pyrene-based derivatives, and the electronic structures, spin-orbit couplings, transition dipole moments, and vibronic couplings have been investigated by theoretical calculations.[19]

Generally, an acetylene group is the preferred choice to extend the π-conjugation of molecular skeletons, due to the development of the efficient Sonogashira coupling reaction. Previously, in our laboratory, we synthesized cruciform-shaped and hand-shaped architectures incorporating π-conjugated alkynylpyrenes as highly efficient blue emissive materials by the Sonogashira cross-coupling reaction.[20,21] The optical properties of both types of pyrene-based material exhibited pure blue fluorescence with good quantum yield, as well as similar crystal packing in the solid-state. Our recent report on the synthesis of 1,3-dibromo-7-*tert*-butylpyrene (**1**)[22] prompted us to further explore 1,3-bis(arylphenyl)pyrenes as blue emissive materials. The arylphenyl groups located at the 1,3-positions were twisted by a considerable angle relative to the pyrene core, a feature that can play a curial role in hindering intermolecular interactions in the solid-state. In this article, a series of *Y*-shaped, extended π-conjugated pyrene derivations have been synthesized by a Pd-catalyzed Sonogashira cross-coupling reaction using 1,3-dibromo-7-*tert*-butylpyrene and corresponding arylethynyl groups in reasonable yield. We anticipated that the extended π-conjugated pyrene derivatives would exhibit interesting topological structures, leading to attractive photophysical properties, as well being air-stable. Indeed, the designed π-conjugated molecules showed interesting CT characteristics in polar solvents as expected. Furthermore, we investigated the effect of the various

substituents and substitution positions of the (arylethynyl)pyrenes for optical properties and crystal packing.

2. Results and Discussion Sections

2.1 Synthesis and characterization

The synthesis of the *Y*-shaped arylethynyl-substituted pyrenes **2** are shown in Scheme 1. The target arylethynyl pyrenes **2** were obtained in 32-67% yield through a Sonogashira coupling reaction between **1** and the corresponding arylacetylenes. All of the new pyrene derivatives **2** have been characterized by $^{1}H/^{13}C$ NMR spectroscopy (Figure S1), HR-MS and elemental analysis. *Y*-shaped compounds **2** with arylethynyl groups display good air-stability and solubility properties in common solvents, such as dichloromethane (CH_2Cl_2), *N*,*N*-dimethylformamide (DMF), tetrahydrofuran (THF) and methanol (CH_3OH). Moreover, the structures of **2c** (two polymorphs), **2d** and **2f** were further confirmed by X-ray single crystal diffraction. The effect of the substituents on the crystal packing, photophysical properties and electrochemistry has been investigated in detail; for comparison, two position-dependent arylethynyl-functionalized pyrenes **3** and **4** are illustrated in Scheme 1. This work allows us to more fully understand the effect of the various substituents and the relationship between molecular structure and optical properties.

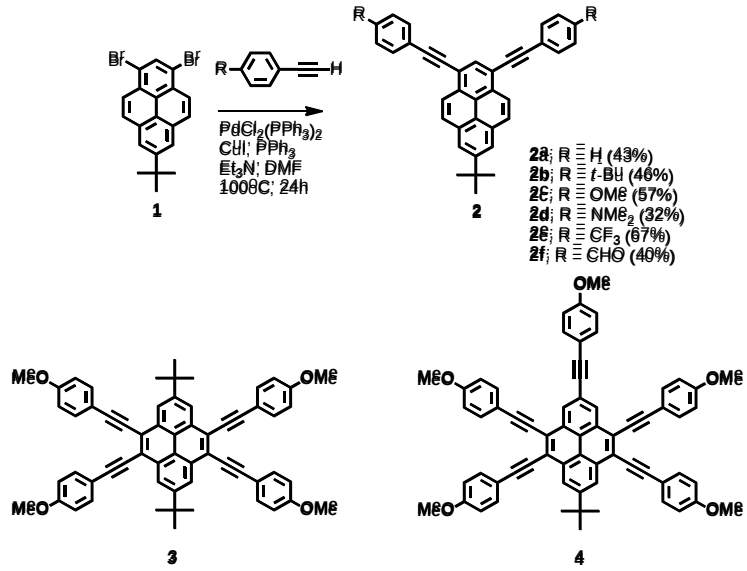

Scheme 1. The synthetic route to π-conjugated pyrene derivatives **2**, and the cruciform-shaped and hand-shaped pyrenes **3** and **4** for comparison.

2.2 Single crystal X-ray crystallography

Single crystals of the extended π-conjugated *Y*-shaped pyrene derivatives **2c** were obtained from MeOH/$CHCl_3$ or hexane/ CH_2Cl_2, **2d·$CHCl_3$** from $CHCl_3$ and **2f** from CH_2Cl_2/benzene by slow evaporation at room temperature. All of the compounds crystallize in the *triclinic* crystal system with space group $P\ \bar{1}$. Compound **2c** was obtained as two different polymorphs, **2cI** with one molecule in the asymmetric unit and **2cII** with two. The molecular structures are shown in Figure 1 and Figure S2 and the crystallographic data is listed in Table **1**.

Table 1. Summary of crystal data for the π-conjugated molecules **2cI**, **2cII**, **2d·$CHCl_3$** and **2f**

Complex	**2cI**	**2cII**	**2d**	**2f**
Empirical formula	$C_{38}H_{30}O_2$	$C_{38}H_{30}O_2$	$C_{40}H_{36}N_2$·CHCl	$C_{38}H_{26}O_2$
Formula weight	518.62	518.62	664.07	514.59
Crystal system	Triclinic	Triclinic	Triclinic	Triclinic
Space group	$P\ \bar{1}$	$P\ \bar{1}$	$P\ \bar{1}$	$P\ \bar{1}$
a[Å]	8.926(2)	8.902(2)	10.8101(12)	8.9354(5)
b[Å]	12.408(3)	12.088(3)	11.1244(12)	11.8785(9)
c[Å]	13.559(3)	27.070(8)	14.3383(16)	13.0754(6)
α[°]	99.758(9)	101.774(18)	91.4712(18)	97.029(5)
β[°]	100.102(9)	93.904(19)	91.6750(18)	102.787(4)
γ[°]	98.809(8)	100.502(18)	101.8031(17)	100.349(5)
Volume[$Å^3$]	1430.9(6)	2787.1(13)	1686.2(3)	1312.22(14)
Z	2	4	2	2
λ	0.71073	1.54184	0.71073	1.54184
Dcalcd[Mg/m^3]	1.204	1.236	1.308	1.302
temperature [K]	293(2)	296(2)	150(2)	100(2)
measured reflns	12587	36576	19720	7853
unique reflns	4927	9802	9976	5075
obsd reflns	2470	4722	7491	3892
Parameters	362	731	552	462
R(int)	0.0337	0.0548	0.0184	0.0219
$R[I> 2\sigma(I)]$[a]	0.0774	0.0887	0.0457	0.0545
*wR*2[all data][b]	0.2342	0.2725	0.1344	0.1687
GOF on F^2	1.007	1.010	1.059	1.052

[a] Conventional *R* on F_{hkl}: $\Sigma||F_o|-|F_c||/\sigma|F_o|$. [b] Weighted *R* on $|F_{hkl}|^2$: $\Sigma[w(F_o^2 - F_c^2)^2]/\Sigma[w(F_o^2)^2]^{1/2}$

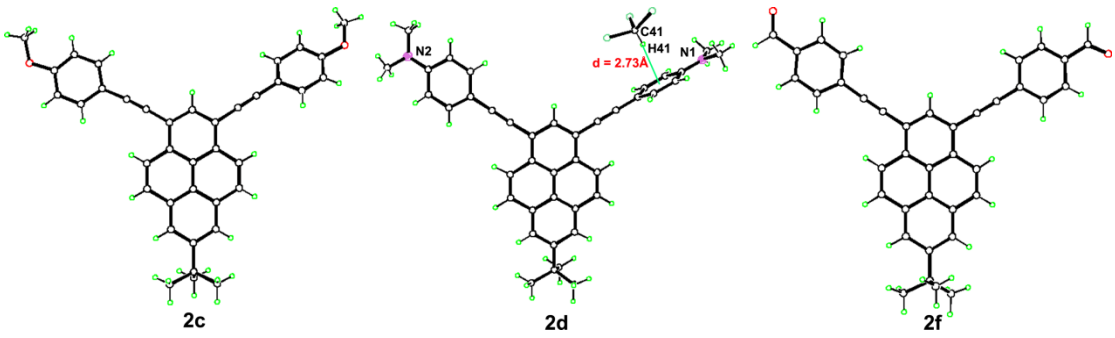

Figure 1. The molecular structures of **2cI**, **2d·CHCl$_3$** and **2f**.

As shown in Figure 2, the structure of **2cI** displays face-to-face π-stacking at a distance of 3.54 Å, which involves 14 carbons in each pyrene molecule.[23] One ethynylphenyl substituent is coplanar with the pyrene core, whilst another forms a twist angle of 28.4°. A number of π···π stacking interactions between the phenyl rings and the neighbouring pyrene core were observed (3.32 Å). In addition, another weak but important interaction involves the methoxyl group, which has a contact with the next layer of the ethynyl fragment of pyrene via a C–H···π interaction (2.42 Å).

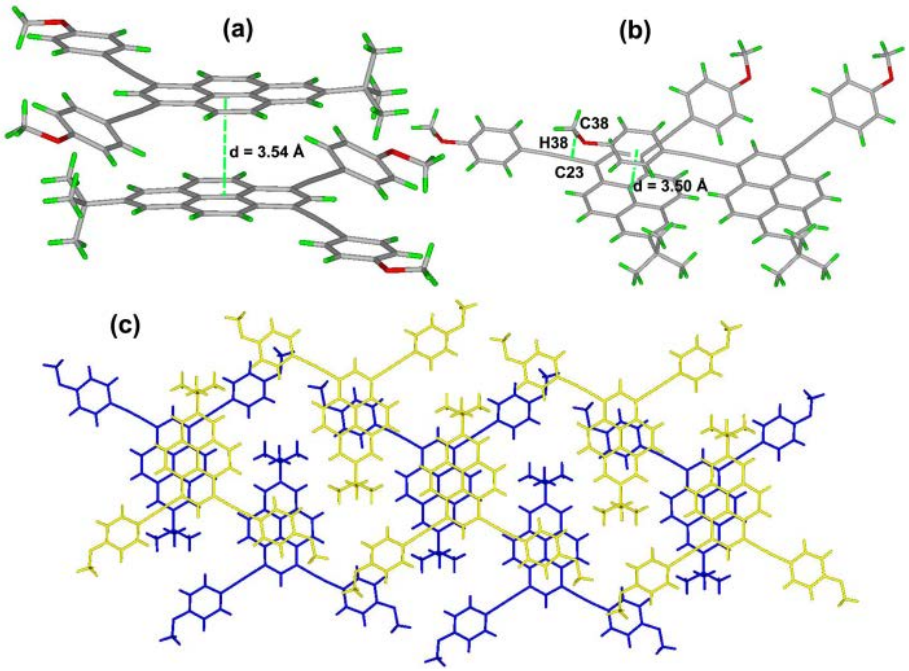

Figure 2. X-ray crystal structure representations of **2cI**, illustrating (**a**) and (**b**) the co-facial π-stacking structures and (**c**) the principal intermolecular packing interactions.

Similarly, the polymorph **2cII** was crystallized from hexane/CH_2Cl_2 solution , The X-ray structure determination revealed that **2cII** crystallises in the same space group

as **2cI**. The crystal packing analysis shows that polymorph **2cII** was arranged similarly to **2cI**. There is a fine dinstinction between the two polymorphs in that the asymmetric unit of **2cII** contained two molecules, whereas that of **2cI** contained only one. (See supporting information)

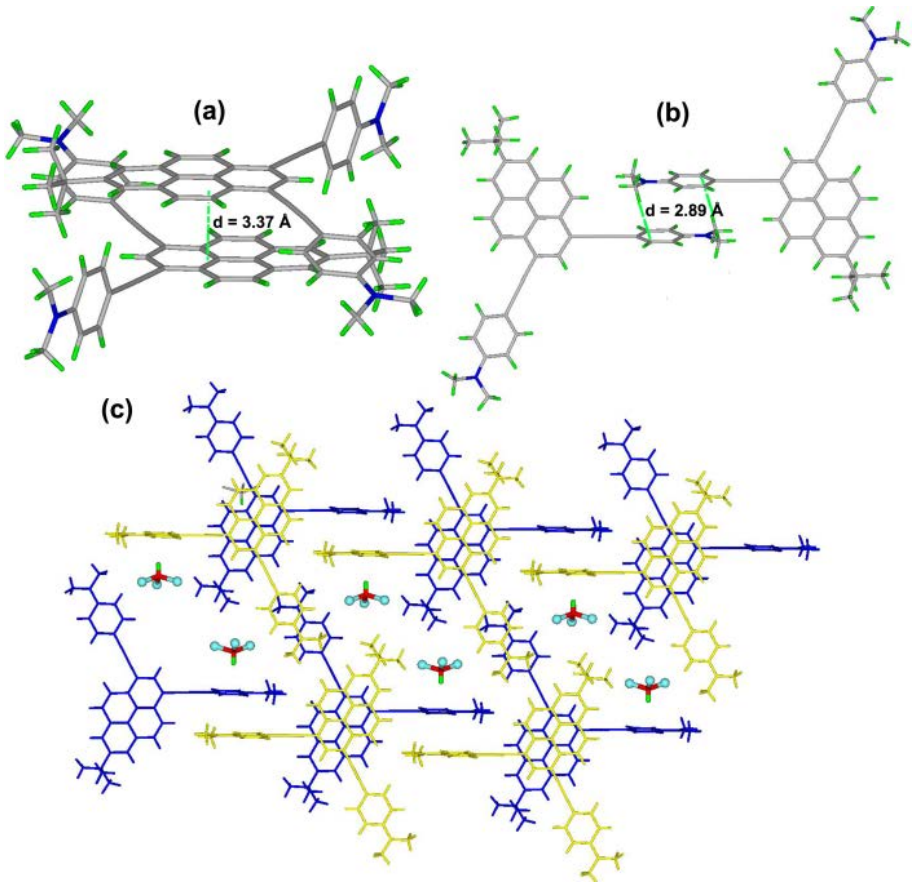

Figure 3. X-ray crystal structure representations of **2d·CHCl$_3$**, illustrating (a) and (b) the co-facial π-stacking structures and (c) $CHCl_3$ molecules were captured in voids supported by C–H···π interactions.

Figure 3 reveals that the asymmetric unit contains a molecule of **2d** and a chloroform linked by a C–H···π interaction at a distance of 2.41(2) Å. Unlike the situation above for **2cI**, where the *p*-methoxylphenylethynyl moieties and the pyrene ring are almost coplanar, here for **2d**, the torsional angle between the pyrene unit and one of the the 4-(*N*,*N*-dimethylamino)phenylethynyl fragments is close to perpendicular with a twist angle of 87.87(3)^o. Moreover, two neighbouring pyrene moieties are present with displaced face-to-face patterns forming a star-shaped architecture in the solid-state; the π···π stacking interactions are approximately 3.37 Å

(Fig 3a). In addition, there are weak π···π stacking interactions between the terminal phenyl groups of neighbouring molecules at nearly 3.50 Å (Figure **3b**).

From the packing pattern, a two-dimensional supramolecular network was constructed by these complicated π···π stacking interactions, and the $CHCl_3$ molecules were captured in the molecular voids[24] by C–H···π interactions.

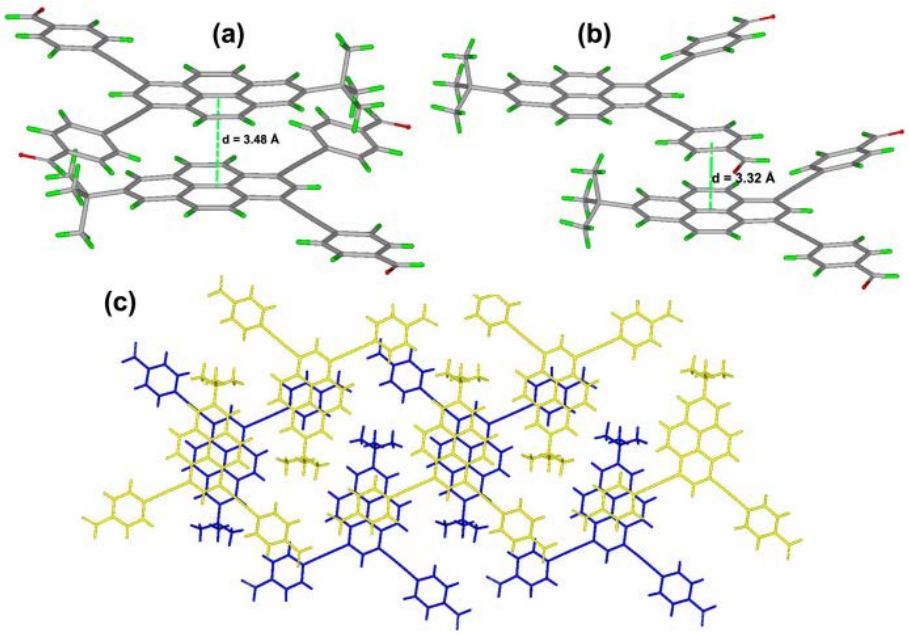

Figure 4. X-ray crystal structure representations of **2f**, illustrating (a) and (b) the detail of the cofacial π-stacking structures and (c) the principal intermolecular packing interactions.

The asymmetric unit of **2f** contains one molecule with no solvent of crystallisation. As shown in Figure 4, **2f** displays a slightly curved core structure (torsional angle <5^o) with shallow twist angles of 17.57(9) and 3.03(8)° between the pyrene core and the terminal phenyl groups. As we predicted, the planar molecular structure would tend to form strong co-facial π···π stacking, and the pairs of pyrene units arrange in head-to-tail stacking via a centre of symmetry by π···π interactions (3.48 Å). In addition, the pyrene units and the adjacent phenyl rings display face-to-face π···π stacking at a distance of 3.32 Å. Interestingly, from the packing structure of **2f**, there are two key π···π interactions leading to a three dimensional infinite supramolecular array.

Previously, the 4,5,9,10-tetrakis[(4-*tert*-butylphenyl)ethynyl]pyrene **3**[20] and

4,5,7,9,10-pentakis[(4-methoxyphenylethynyl)]pyrene **4**[21] were prepared successfully by our group, that allowed us to further compare the effect of the substituent number or the position of arylethynyl moieties on the crystal arrangement. In the packing structure of **3**, the four phenyl rings are not coplanar with and the central pyrene; the two unique dihedral angles are 18.3 and 23.6°. As shown in Figure 5, two neighbouring pyrene moieties possess a centroid-to-centroid distance of 5.99 Å. No significant π-stacking interactions between the pyrene rings were observed and molecules adopt a herringbone packing motif. Non-covalent interactions play an important role in the stacking of the structures.

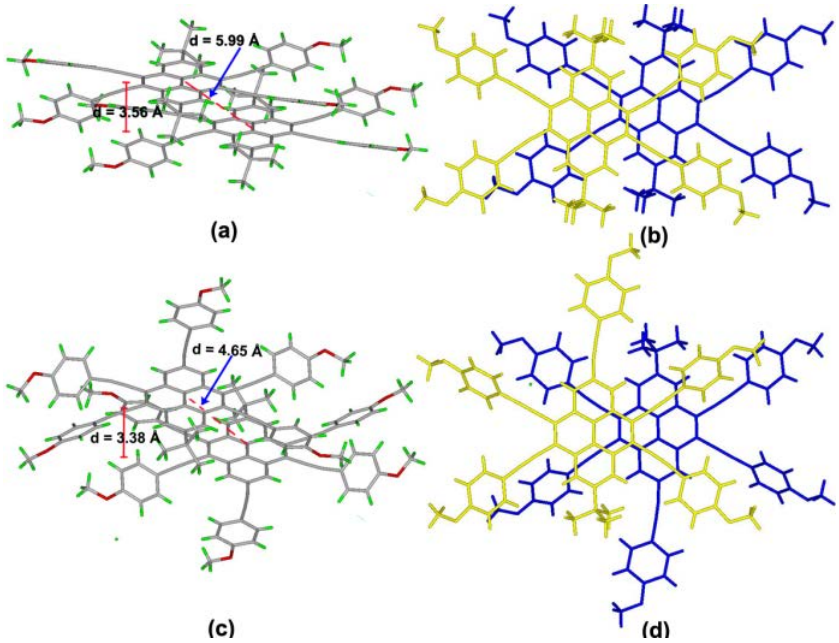

Figure 5. The packing structure (a) side view and (b) top view for **3** and (c) side view and (d) top view for **4**.

However, in compound **4,** when a *p*-methoxyphenyl moiety is located at the 7-position of pyrene, it is almost coplanar with the pyrene ring. The other four phenyl rings at the 4,5,9,10-positions of the pyrene form dihedral angles of between 6.1 and 47.3°, and two neighbouring pyrene moieties adopt a slipped face-to-face motif with off-set head-to-tail stacking with a centroid-to-centroid distance of 4.65 Å. Each molecule of **4** displays 24-point π-π stacking with molecules above and below using both the pyrenyl and ethynyl carbons with intermolecular distances of 3.42-3.58 Å.

As mentioned above, comparing the bis(1,3-substituted) pyrenes **2**, tetra-(4,5,9,10-substituted) and penta(4,5,7,9,10-substituted) pyrenes **3** and **4**, the molecular packing of the arylethynyl-substituted pyrene derivatives have been strongly influenced by either varying the substituent number or substitution position. With the substituted group number increasing, the crystal packing has been transformed from face-to-face π···π stacking with off-set head-to-tail stacking to a herringbone arrangement on going from **2**, **3** to **4**. On the other hand, bulkier *tert*-butyl groups located at the 7-position of pyrene can play a more crucial role in hindering the π···π stacking *versus* the arylethynyl-substituted group. In compound **4**, due to the nodal planes passing through the 7-position of the pyrene, the phenyl moiety attached at this position would be of limited impact for the crystal arrangement, as well as the electronic interactions.[25] The planar molecular structure of the pyrene derivatives **2**, **3** and **4** is beneficial for extending π-conjugation and improving the optical density, which can lead to special photophysical properties both in solution and in the solid state.

2.3 Photophysical properties

The absorption spectra of the title compound **2** in dilute dichloromethane are presented in Figure 6 and the optical data is summarized in Table 2. The maximum absorption wavelength of the ethynylpyrenes is exhibited at *ca*. 68 nm red-shifted compared with 2-*tert*-butyl pyrene (338 nm).[15] Notably, the photophysical properties are highly dependent on the substituent units present. *Y*-shaped **2a**-**c** and **2e** show similar absorption behaviour and exhibit two prominent absorption bands in the regions 300-350 nm and 375-425 nm respectively. For **2d** and **2f**, the maximum absorption wavelength has obviously red-shifted (~19nm) relative to **2a**, arising from the intramolecular charge transfer (ICT) increase. Indeed, both **2d** and **2f** feature a broader and intense absorption in the long wavelength region 475-525 nm, indicating that the molecules tend to be more coplanar between the pyrene core and terminal ethynylphenyl groups by extending the π-conjugation, which is consistent with the crystallographic results. With an increased length of π-conjugation, the molar

absorption coefficients (**ε**) of **2d** and **2f** are lower than the others observed.

Table 2. The photophysical and electrochemical properties of compounds **2**.

R	$\lambda_{max\ abs}$ [a] nm	$\lambda_{max\ PL}$ [a] (nm)	Log ε ($M^{-1}\cdot cm^{-1}$)	Φ_f [a]	LUMO (eV)	HOMO (eV)	Energy gap (eV)	ι ns	T_m [f]	T_d [g]
2a	406	421 (325)	4.87	0.93	–2.01b (–2.41)c	–5.01b (–5.34)d	2.99b (2.93)e	2.89a	198	479
2b	409	423 (330)	4.88	0.93	–1.93 (–2.39)	–4.93 (–5.31)	2.99 (2.92)	2.93	288	469
2c	412	427 (333)	4.82	0.94	–1.85 (–2.37)	–4.79 (–5.27)	2.94 (2.90)	2.94	195	449
2d	431	517 (380)	4.74	0.86	–1.63 (–2.61)	–4.46 (–5.27)	2.83 (2.67)	3.51	237	440
2e	411	427 (313)	4.80	0.91	–2.37 (–2.42)	–5.33 (–5.32)	2.97 (2.90)	2.48	220	469
2f	425	485 (363)	4.77	0.80	–2.56 (--)	-5.39 (--)	2.83 (2.77)	nd	nd	nd

[a] Measured in dichloromethane at room temperature.[b] DFT/B3LYP/6-31G* using Gaussian. [c] Calculated from the empirical formulae HOMO = -(E_{ox}+4.8), [d] LUMO=HOMO+E_g, [e] Calculated from λ_{edge}, [f] Melting temperature (T_m) obtained from differential scanning calorimetry (DSC) measurement. [g] Decomposition temperature (T_d) obtained from thermogravimetric analysis (TGA), nd: not measured.

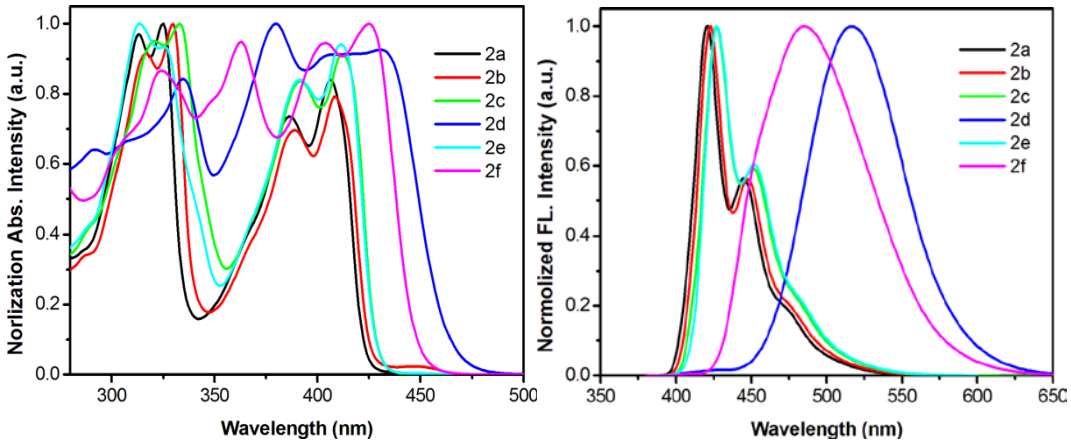

Figure 6. (a) Normalized UV-vis absorption and (b) fluorescence emission spectra of compounds **2** recorded in dichloromethane solutions at ~10^{-5}-10^{-6} M at 25 °C.

The fluorescence spectra of **2a-c** and **2e** exhibit a sharp peak at $\lambda_{em\ max}$ 421, 423, 427 and 427 nm with a shoulder. The emission spectra of **2d** and **2f** exhibit a single broad peak at 517 nm and 485 nm, respectively, which indicates that the emission occurs from the lowest excited state with the largest oscillator strength. With the π-conjugation increasing, a gradual bathochromic shift in the $\lambda_{em\ max}$ is clearly observed in the order of **2a** ≈ **2b** ≈ **2c** ≈ **2e** < **2f** < **2d**, implying that the energy gap between ground and excited states would decrease in this order. In this process, the ICT plays an important role in lowering the energy gap.[18,26] All of compounds show strong emission from deep blue to green color with high PL quantum yield (QYs) in

the 0.80-0.94 range. Additionally, the fluorescence lifetime (τ_s) were measured in chloromethane, and the results are listed in Table 2.

Furthermore, the effect on the optical properties of these compounds has been examined in solvents of various polarity, such as cyclohexane, 1,4-dioxane, tetrahydrofuran (THF), dichloromethane (DCM) and *N*,*N*-dimethylformamide (DMF). (Figure S3) The solvent dependence of the absorption and fluorescene spectra of **2** are displayed in Figure 7 and in the supporting information. The fluorescence spectra of **2d** and **2f** showed an obvious intermolecular charge transfer (ICT) emission band in different polarity solvents; for example, in **2d**, there was a remarkable solvatochromic color change from blue (432 nm in cyclohexane) to yellow (560 nm in DMF), owing to the presence of the terminal electron-donating *N*,*N*-dimethylamino groups (-N(CH_3)$_2$) which lead to a large singlet excited-state dipole moment.[27] The solvent effect of the absorption and fluorescence spectra was further evaluated by the Lippert-Mataga plot (Eqs. (1)-(2)),[28] which is dependent on the Stokes shift ($\Delta\nu_{st}$) and the solvent parameter $\Delta_f(\varepsilon, n)$.[29]

$$\Delta\nu = \frac{1}{4\pi\varepsilon_0 hc a^3}\ \frac{2\Delta\mu^2}{hcR^3}\ \Delta f + \text{const} \qquad (1)$$

Where $\Delta\nu = \nu_{abs} - \nu_{em}$ stands for Stokes shift, ν_{abs} is the wavenumber of maximum absorption, ν_{em} is the wavenumber of maximum emission, $\Delta\mu = \mu_e - \mu_g$ is the difference in the dipole moment of solute molecule between excited (μ_e) and ground (μ_g) states, *h* is the Planck's constant, R is the radius of the solvent cavity in which the fluorophore resides (Onsager cavity radius), and Δf is the orientation polarizability given by (Eq. 2)

$$\Delta f = \frac{\varepsilon - 1}{2\varepsilon + 1} - \frac{n^2 - 1}{2n^2 + 1} \qquad (2)$$

Where ε is the static dielectric constant and n the refractive index of the solvent.

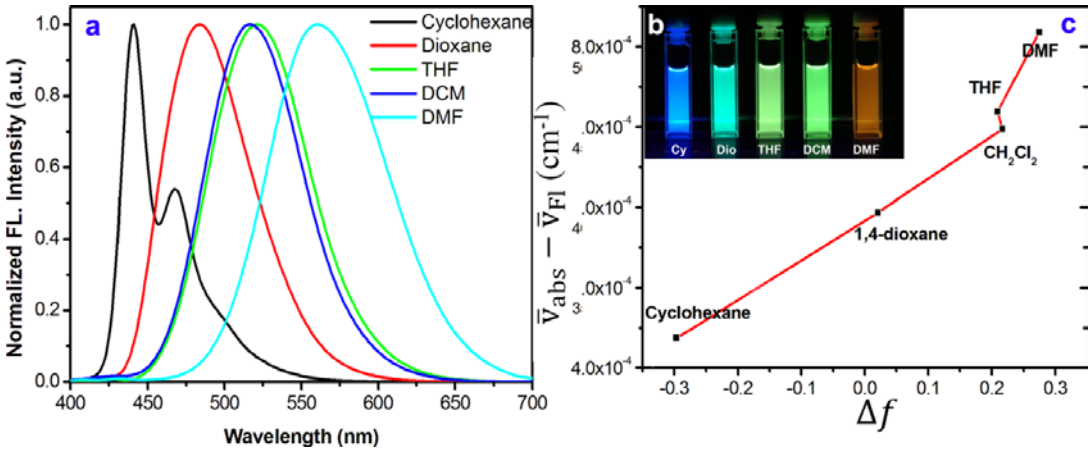

Figure 7. (a) Emission spectra of **2d** in cyclohexane, THF, CH_2Cl_2, CH_3CN and DMF at 25 °C. (b) the solvatochromic colour change from blue to yellow, (c) Lippert-Mataga plots for compound **2d** ($-N(CH_3)_2$).

Similarly, the fluorescence spectra of **2f** show ICT characteristics, and the maximum emission wavelength is red shifted *ca*. 76 nm from 432 nm in cyclohexane to 497 nm in DMF. However, the pyrene derivatives **2a-c** and **2e** show very weak solvatochromic behaviour even in DMF (see supporting information). Although the compounds possess weak CT characteristics, they display relatively high QYs compared with the others.

2.4 Electrochemical properties

The electronic properties of the title compounds **2a-e** were investigated by cyclic voltammetry (CV) in dichloromethane containing 0.1 M nBu_4NPF_6 as the supporting electrolyte, with a scan rate of 100 mVs^{-1} at room temperature. As shown in Figure 8, all of the *Y*-shaped extended π-conjugated pyrene derivatives displayed an irreversible oxidation peak. In contrast, previous studies on similar *Y*-shaped pyrene molecules with aryl-substituted moieties have shown a quasi-reversible oxidation wave,[22] which might be due to the terminal nature of the π-conjugated arylethynyl substitution effect on the electronic properties. For **2a-e**, the CV peaks for the positive potentials range from 1.23 to 1.28 V. According to the CVs and the UV-vis absorption, the highest occupied molecular orbital (HOMO) were estimated from the onset values of the first oxidation, and the optical energy gap (E_g) was derived from the UV-vis data. The

HOMO energy levels for **2a-e** ranged from –5.28 to –5.34 eV, followed the empirical formula LUMO = HOMO-E_g, the LUMO levels of **2a-e** are located from –2.37 to –2.61 eV. Given the considerable HOMO and LUMO energy values of the compound, it might have potential use as a luminescent hole-transporting material in OLEDs.[30]

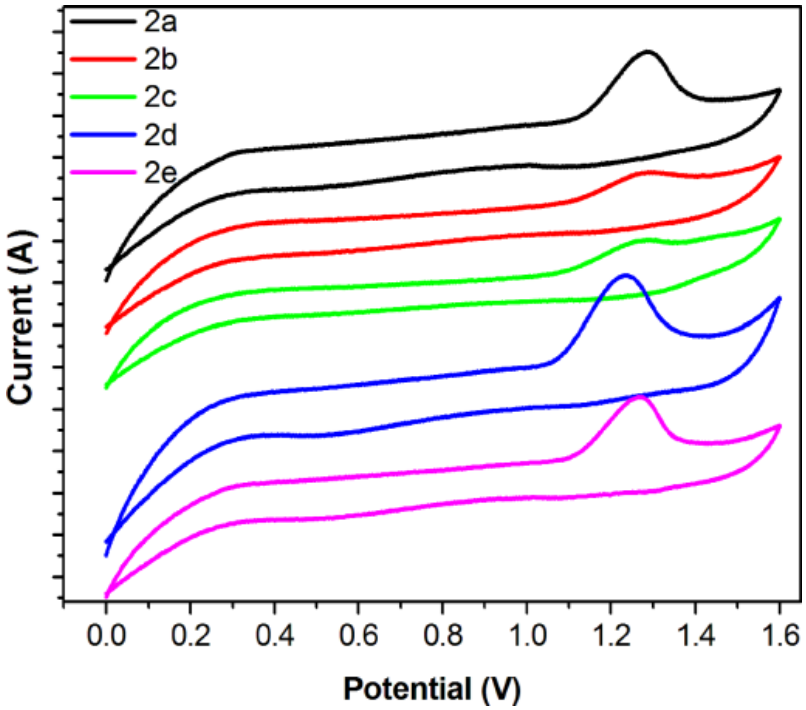

Figure 8. Cyclic voltammograms recorded for compounds **2a-e**.

2.5 Quantum chemistry calculations

To gain further insight into the electronic structures of the Y-shaped π-conjugated compounds **2**, DFT calculations were performed at the B3LYP/6-31G(d) level of theory using the Gaussian 2003 program.

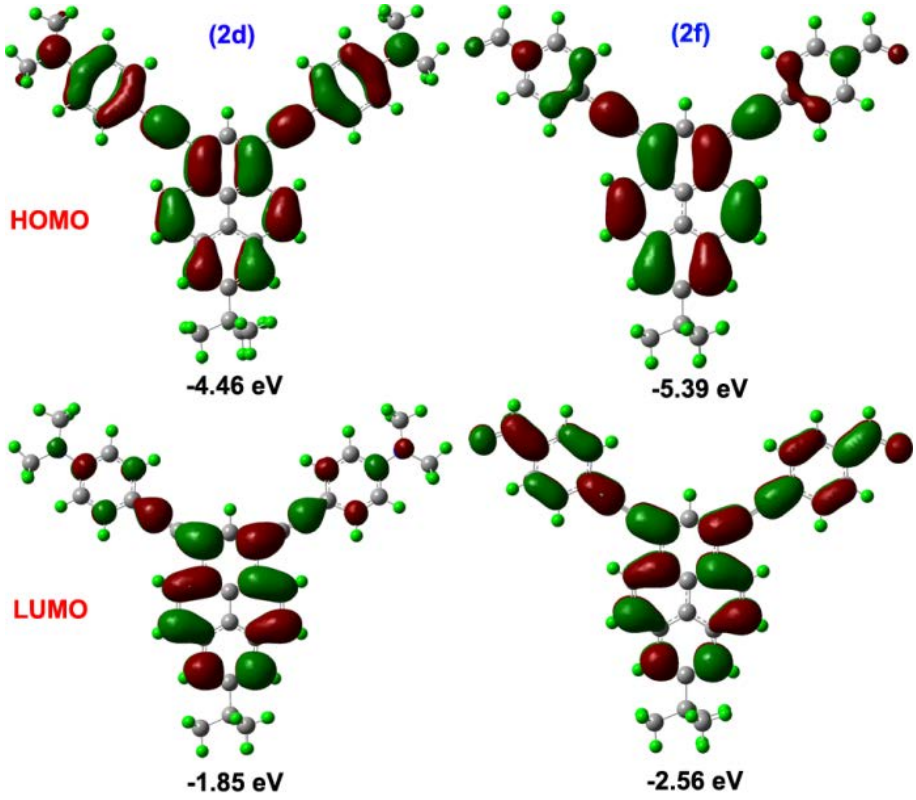

Figure 9. Selected computed molecular orbital plots (B3LYP/6-31G*) of the compounds **2d** and **2f**.

The 3D-structures and energy density of the HOMO and LUMO levels of each material are displayed in Figure 9 and in the supporting information Figure S4. As the molecular geometries show, the substituent groups are almost coplanar with the pyrene core. Thus there is a close correlation between the quantum calculations and the results from the single crystal X-ray diffraction results; minor differences of molecular geometry arise from the theoretical calculations being carried out in the "gas-phase". On the other hand, the various substituent groups play a significant role for the HOMOs and LUMOs, for example, as the electron-releasing ability increases from **2a** to **2d**, the destabilization of the HOMOs is greater than that of the LUMO, the HOMO levels are mostly located over the full molecular skeleton, whereas the LUMOs only spread in the center of pyrene rings; in contrast, with electron-withdrawing moieties, the LUMOs of **2e** and **2f** are almost fully localized on the entire molecular framework, and the HOMOs destabilized in the pyrene ring and a fragment of the phenyl groups. In addition, from the calculation data, we observed the

energy gap of **2f** is close to **2d** with 2.83 eV, so both compounds exhibit similar UV spectra with a broad and strong absorption band in the 370-450 nm region. It is noteworthy that the HOMO-LUMO energy gaps of the title compounds **2** are lower than that previously reported for *Y*-shaped 1,3-bisaryl-functionalized pyrene species,[22] due to the effect of arylethynyl moieties on the energies of the molecular orbitals.

Conclusions

In summary, a series of *Y*-shaped arylethynyl-functionalized pyrenes **2** were synthesized by Pd-catalyzed Sonogashira coupling reaction in reasonable yield. The *Y*-shaped, extended π-conjugated pyrene derivatives display strong face-to-face π-stacking with off-set head-to-tail stacking as compared with a *Y*-shaped carbon-carbon single bond arylsubstituted pyrene.[22] Furthermore, the effects of the substituents and their position on the crystal packing structure and photophysical properties of the chromophores has been evaluated. Compounds **2a-c** and **2e** in dichloromethane exhibited deep blue fluorescence with high quantum yield, while the chromophores **2d** and **2f** exhibit interamolecular charge-transfer (ICT) leading to intense optical absorbances over a wide spectral range. Strong fluorescence spectra of 2d and 2f show the maximum emission at 517 nm and 485 nm respectively, with remarkable solvatochromic effects in polar solvents. Theoretical computation and experimental CV studies on their electrochemistry verify that *Y*-shaped extended π-conjugated pyrenes **2** can be utilized in OLED devices as luminescent hole-transporting materials. In future, we will attempt to fabricate highly efficient OLED devices using these materials.

Experimental Section

General procedures

All melting points (Yanagimoto MP-S1) are uncorrected. ^{1}H NMR spectra (300 MHz) were recorded on a Nippon Denshi JEOL FT-300 NMR spectrometer and ^{13}C NMR spectra (400 MHz) were recorded on an Agilent NMR System 400 spectrometer,

and referenced to 7.26 and 77.0 ppm respectively for chloroform-D solvent with $SiMe_4$ as an internal reference: *J*-values are given in Hz. IR spectra were measured for samples as KBr pellets in a Nippon Denshi JIR-AQ2OM spectrophotometer. UV-vis spectra were recorded on a Perkin Elmer Lambda 19 UV/VIS/NIR spectrometer. Mass spectra were obtained on a Nippon Denshi JMS-01SA-2 spectrometer at 75 eV using a direct-inlet system. Elemental analyses were performed by Yanaco MT-5. Elemental analyses were performed by Yanaco MT-5. The fluorescence quantum yield and fluorescence lifetime is calibrated by the ratio of the number of photons emitted to the number of photons absorbed and were measured (Edinburgh, FL920) in solution using the integrated sphere absolute PL quantum yield measurement method.[31] Thermogravimetric analysis (TGA) was undertaken using a NETZSCH TG 209 under nitrogen atmosphere at a heating rate of 10 °C min^{-1}. The geometries of all the compounds were calculated by density functional theory (DFT) methods using the B3LYP/6-31G* function.

Crystallography.

Crystallographic data are summarized in Table 1. Data were collected on A Bruker SMART APEX CCD diffractometer for **2cI**,[32] a Rigaku R-AXIS RAPID image plate diffractometer for **2cII**,[33] a Bruker APEX 2 CCD diffractometer for **2d**,[32] and an Agilent SuperNova with Atlas CCD diffractometer for **2f**.[33] ω-scans were employed. Data were corrected for Lorentz and polarisation effects and for absorption.[32,33] The structures were solved by charge flipping or direct methods algorithms and refined by full-matrix least-squares methods, on F^2.[34,35] Data (excluding structure factors) on the

structures reported here have been deposited with the Cambridge Crystallographic Data Centre with deposition numbers. CCDC 1430528–30 & 1453069 for **2cI**, **2cII**, **2d**, and **2f**, CCDC 713975 for **3**, and CCDC 811807 for **4**, contain the supplementary crystallographic data for this paper. These data can be obtained free of charge from The Cambridge Crystallographic Data Centre via www.ccdc.cam.ac.uk/data_request/cif.

Materials: Unless otherwise stated, all other reagents used were purchased from commercial sources and used without further purification. The preparation of 1,3-dibromo-7-*tert*-butylpyrene (**1**) has been described previously.[22]

Synthesis of 1,3-bisarylethynyl-7-*tert*-butylpyrenes (2)

The series of compounds **2** was synthesized from 1,3-dibromo-7-*tert*-butylpyrene **(1)** with the corresponding arylethynyl compound by a Sonogashira coupling reaction.

Synthesis of 7-*tert*-butyl-1,3-bis(4-methoxyphenylethynyl)pyrene (2c)

To a stirred solution of 1,3-dibromo-7-*tert*-butylpyrene (**1)** (200 mg, 0.481 mmol), in Et_3N (10 mL) and DMF (10 mL), was added 4-methoxyphenyl acetylene (254 mg, 1.92 mmol) and PPh_3 (20.0 mg, 0.077 mmol), and the mixture was stirred at room temperature under argon. $PdCl_2(PPh_3)_2$ (24 mg, 0.034 mmol), CuI (10 mg, 0.053 mmol) were then added, and the mixture was heated to 100 °C with stirring for 24 h. After it was cooled, the mixture was diluted into CH_2Cl_2 (50 mL) and washed successively with saturated aqueous $NH_4Cl{\cdot}H_2O$ and brine. The mixture was extracted with dichloromethane (40 mL × 2), after washed with water and brine. The combined organic extracts were dried with anhydrous $MgSO_4$ and evaporated. The residue was purified by column chromatography eluting with CH_2Cl_2-hexane (1:1) to give 7-*tert*-butyl-1,3-bis(4-methoxyphenylethynyl)pyrene **2c** as a light yellow solid. Recrystallization from hexane gave **2c** (142 mg, 57 %) as a light yellow solid. M.p. 191-192 °C. IR ν_{max} (KBr)/cm^{-1}: 1591, 1513, 1457, 1288, 1249, 1166, 1029, 872, 822,

714 and 530. ^{1}H NMR (300 MHz, $CDCl_3$) δ_H = 1.60 (s, 9H, *t*Bu), 3.87 (s, 6H, OMe), 6.96 (d, *J* = 9.0 Hz, 4H, Ar-*H*), 7.66 (d, *J* = 9.0 Hz, 4H, Ar-*H*), 8.15 (d, *J* = 9.2 Hz, 2H, pyrene-*H*), 8.26 (s, 2H, pyrene-*H*), 8.36 (s, 1H, pyrene-*H*) and 8.59 (d, 2H, *J* = 9.0 Hz, pyrene-*H*) ppm. ^{13}C NMR (100 MHz, $CDCl_3$): δ_C = 31.90, 35.28, 55.38, 86.82, 95.16, 114.18, 115.61, 117.93, 122.42, 123.29, 124.48, 125.43, 128.88, 131.18, 131.27, 132.57, 133.22, 149.72 and 159.86 ppm. FABMS: *m/z* calcd for $C_{38}H_{30}O_2$ 518.22 [M^+]; found 518.09 [M^+]. Anal. calcd for $C_{38}H_{30}O_2$ (518.64): C 88.00, H 5.83%. Found: C 87.89, H 5.63%.

A similar procedure using phenylacetylene, 4-*tert*-butylphenylacetylene, *N*,*N*-dimethyl-4-ethynylaniline, 4-(trifluoromethyl)phenylacetylene and 4-ethynylbenzaldehyde was followed for the synthesis of **2a**, **2b**, **2d-f**.

7-*tert*-Butyl-1,3-bisphenylethynylpyrene (2a) was obtained as a light green solid (recrystallized from hexane, 95 mg, 43%). M.p. 182-183 °C. IR ν_{max} (KBr)/cm^{-1}: 3046, 2957, 1600, 1587, 1513, 1487, 1443, 1379, 1355, 1225, 1153, 891, 876, 813, 752, 716, 687 and 534. ^{1}H NMR (300 MHz, $CDCl_3$) δ_H = 1.60 (s, 9H, *t*Bu), 7.37-7.47 (m, 6H, Ar-*H*), 7.71-7.74 (m, 4H, Ar-*H*), 8.18 (d, *J* = 9.2 Hz, 2H, pyrene-*H*), 8.28 (s, 2H, pyrene-*H*), 8.40 (s, 1H, pyrene-*H*) and 8.61 (d, *J* = 9.2 Hz, 2H, pyrene-*H*) ppm. ^{13}C NMR (100 MHz, $CDCl_3$): δ_C = 31.90, 35.30, 88.02, 95.13, 117.52, 122.34, 123.45, 123.52, 124.41, 125.33, 128.51, 129.21, 131.12, 131.65, 131.75, 132.88 and 149.83 ppm. FABMS: *m/z* calcd for $C_{36}H_{26}$ 458.20 [M^+]; found 458.08 [M^+]. Anal. calcd for $C_{36}H_{26}$ (458.59): C 94.29, H 5.71%. Found: C 94.09, H 5.91%.

7-*tert*-Butyl-1,3-bis(4-*tert*-butylphenylethynyl)pyrene (2b) was obtained as light green needles (recrystallized from hexane, 126 mg, 46%). M.p. 298-299 °C. IR ν_{max} (KBr)/cm^{-1}: 2959, 1515, 1464, 1360, 1225, 873, 831, 714 and 557. ^{1}H NMR (300 MHz, $CDCl_3$) δ_H = 1.38 (s, 18H, *t*Bu), 1.60 (s, 9H, *t*Bu), 7.46 (d, *J* = 8.4 Hz, 4H, Ar-*H*), 7.66 (d, *J* = 8.6 Hz, 4H, Ar-*H*), 8.16 (d, *J* = 9.2 Hz, 2H, pyrene-*H*), 8.27 (s, 2H, pyrene-*H*), 8.38 (s, 1H, pyrene-*H*) and 8.61 (d, *J* = 9.0 Hz, 2H, pyrene-*H*) ppm. ^{13}C NMR (100 MHz, $CDCl_3$): δ_C = 31.23, 31.90, 34.90, 35.28, 87.42, 95.30, 117.79, 120.43, 122.39, 123.38, 124.44, 125.41, 125.51, 129.02, 131.16, 131.50, 132.77,

149.74 and 151.84 ppm. FABMS: *m/z* calcd for $C_{44}H_{42}$ 570.33 [M^+]; found 570.19 [M^+]. Anal. calcd for $C_{44}H_{42}$ (570.80): C 92.58, H 7.42%. Found: C 92.78, H 7.22%.

7-*tert*-Butyl-1,3-bis(4-*N*,*N*-dimethylaminophenylethynyl)pyrene (2d) was obtained as yellow prisms (recrystallized from CH_2Cl_2-hexane (3:7), 84 mg, 32%). M.p. 221-223 °C. IR ν_{max} (KBr)/cm^{-1}: 2189, 1650, 1523, 1441, 1362, 1219, 1178, 1147, 812 and 752. ^{1}H NMR (300 MHz, $CDCl_3$) δ_H = 1.59 (s, 9H, *t*Bu), 3.03 (s, 12H, NMe_2), 6.74 (d, *J* = 9.0 Hz, 4H, Ar-*H*), 7.59 (d, *J* = 9.0 Hz, 4H, Ar-*H*), 8.12 (d, *J* = 9.0 Hz, 2H, pyrene-*H*), 8.23 (s, 2H, pyrene-*H*), 8.33 (s, 1H, pyrene-*H*) and 8.61 (d, *J* = 9.0 Hz, 2H, pyrene-*H*) ppm. ^{13}C NMR (100 MHz, $CDCl_3$): δ_C = 31.91, 35.25, 40.26, 86.27, 96.47, 110.33, 111.97, 118.62, 122.59, 122.94, 124.58, 125.67, 128.39, 130.76, 131.30, 132.26, 132.89, 149.51 and 150.28 ppm. FABMS: *m/z* calcd for $C_{40}H_{36}N_2$ 544.29 [M^+]; found 544.11 [M^+]. Anal. calcd for $C_{40}H_{36}N_2$ (544.73): C 88.20, H 6.66, N 5.14%. Found: C 88.01, H 6.96, N 5.03%.

7-*tert*-Butyl-1,3-bis(4-trifluoromethylphenylethynyl)pyrene (2e) was obtained as light green needles (recrystallized from hexane, 192 mg, 67%). M.p. 241-243 °C. IR ν_{max} (KBr)/cm^{-1}: 1611, 1322, 1161, 1123, 1064, 1015 and 889. ^{1}H NMR (300 MHz, $CDCl_3$) δ_H = 1.61 (s, 9H, *t*Bu), 7.69 (d, *J* = 8.0 Hz, 4H, Ar-*H*), 7.80 (d, *J* = 7.9 Hz, 4H, Ar-*H*), 8.20 (d, *J* = 9.0 Hz, 2H, pyrene-*H*), 8.30 (s, 2H, pyrene-*H*), 8.40 (s, 1H, pyrene-*H*) and 8.56 (d, *J* = 8.9 Hz, 2H, pyrene-*H*) ppm. ^{13}C NMR (100 MHz, $CDCl_3$): δ_C = 31.88, 35.34, 90.24, 93.69, 116.66, 122.16, 122.62, 123.96, 124.31, 125.02, 125.52, 127.13, 129.80, 129.99, 130.31, 130.99, 131.83, 131.89, 131.98, 132.12, 133.16 and 150.11 ppm. FABMS: *m/z* calcd for $C_{38}H_{24}F_6$ 594.18 [M^+]; found 593.65 [M^+]. Anal. calcd for $C_{38}H_{24}F_6$ (594.59): C 76.76, H 4.07%. Found: C 76.86, H 4.27%.

7-*tert*-Butyl-1,3-bis(4-formylphenylethynyl)pyrene (2f) was obtained as a yellow solid (recrystallized from CH_2Cl_2-hexane (3:7), 100 mg, 40 %). M.p. 283-285°C. IR ν_{max} (KBr)/cm^{-1}: 1696, 1600, 1557, 1203, 1163 and 873. ^{1}H NMR (300 MHz, $CDCl_3$) δ_H = 1.61 (s, 9H, *t*Bu), 7.84 (d, *J* = 8.4 Hz, 4H, Ar-*H*), 7.93 (d, *J* = 8.4 Hz, 4H, Ar-*H*), 8.22 (d, *J* = 9.2 Hz, 2H, pyrene-*H*), 8.32 (s, 2H, pyrene-*H*), 8.41 (s, 1H, pyrene-*H*), 8.57 (d, *J* = 9.2 Hz, 2H, pyrene-*H*) and 10.06 (s, 2H, C*H*O) ppm. ^{13}C NMR (100 MHz,

$CDCl_3$): δ_C = 31.88, 35.34, 91.93, 94.32, 116.61, 122.12, 124.08, 124.29, 124.99, 129.54, 129.71, 129.94, 130.96, 132.16, 132.25, 133.25, 135.56, 150.17 and 191.38 ppm. FABMS: *m/z* calcd for $C_{38}H_{26}O_2$ 514.19 [M^+]; found 513.71 [M^+]. Anal. calcd for $C_{38}H_{26}O_2$ (514.61): C 88.69, H 5.09%. Found: C 88.49, H 5.29%.

ASSOCIATED CONTENT

Supporting Information

For crystallographic data in CIF format, $^1H/^{13}C$ NMR data, complete photophysical and electrochemical data, and theoretical data. This material is available free of charge *via* the Internet at http://pubs.acs.org.

AUTHOR INFORMATION

Corresponding Author

E-mail: yamatot@cc.saga-u.ac.jp, hyxhn@sina.com

Notes

The authors declare no competing financial interest.

ACKNOWLEDGMENT

This work was performed under the Cooperative Research Program of "Network Joint Research Center for Materials and Devices (Institute for Materials Chemistry and Engineering, Kyushu University)". We also would like to thank the EPSRC (overseas travel grant to C.R.), The Scientific Research Foundation for the Returned Overseas Chinese Scholars, State Education Ministry and The Scientific Research Common Program of Beijing Municipal Commission of Education for financial support (18190115/008).

REFERENCES

(1) Wang, C.-L.; Dong, H.-L.; Hu, W.-P., Liu, Y.-Q.; Zhu, D.-B. *Chem. Rev.*, **2012**, *112*, 2208-2267.

(2) Usta, H.; Facchetti, A.; Marks, T. *Acc. Chem. Res.*, **2011**, *44*, 501-510.

(3) Pietrangelo, A., Patrick, B. O., MacLachlan, M. J., Wolf, M. O. *J. Org. Chem.*, **2009**, *74*, 4918-4926.

(4) Wu, W., Liu Y.-Q., Zhu, D.-B. *Chem. Soc. Rev.*, **2010**, *39*, 1489-1502.

(5) Li, J., Zhang, Q. *ACS Appl. Mater. Interfaces*, **2015**, *7*, 28049–28062.

(6) Cheng, Y.-J., Yang, S.-H., Hsu, C.-S. *Chem. Rev.*, **2009**, *109*, 5868-5923.

(7) (a) Murphy, A. R.; Fréchet, J. M. J. *Chem. Rev.*, **2007**, *107*, 1066-1096; (b) Mardanya, S., Karmakar, S.; Mondal, D., Baitalik, S. *Dalton Trans.*, **2015**, *44*, 15994- 16012.

(8) Tang, M. L., Mannsfeld, S. C. B., Sun, Y.-S., Becerril, H. A., Bao, Z. *J. Am. Chem. Soc.*, **2009**, *131*, 882-883.

(9) Figueira-Duarte, T. M.; Müllen, K. *Chem. Rev.*, **2011**, *111*, 7260-7314.

(10) Karthik, D., Thomas, K. R. J., Jou, J.-H.; Kumar, S.; Chen, Y.-L., Jou, Y.-C. *RSC Adv.*, **2015**, *5*, 8727-8738.

(11) Chercka, D., Yoo, S.-J., Baumgarten, M., Kim, J.-J., Müllen, K. *J. Mater. Chem. C*, **2014**, *2*, 9083-9086.

(12) Salunke, J. K., Wong, P. S., F. L.; Roy, V. A. L., Lee, C. S., Wadgaonkar, P. P., *Phys. Chem. Chem. Phys.*, **2014**, *16*, 23320-23328.

(13) Jeon, N. J., Lee, J., Noh, J. H., Nazeeruddin, M. K., Grätzel, M., Seok, S. Il. *J. Am. Chem. Soc.*, **2013**, *135*, 19087-19090.

(14) Hu, J.-Y., Feng, X., Seto, N., Do, J.-H., Zeng, X., Tao, Z.; Yamato, T. *J. Mol. Struc.*, **2013**, *1035*, 19-26.

(15) Feng, X., Hu, J.-Y., Iwanaga, F., Seto, N., Redshaw, C., Elsegood, M. R. J., Yamao, T. *Org. Lett.*, **2013**, *15*, 1318-1321.

(16) Diring, S., Camerel, F., Donnio, B., Dintzer, T., Toffanin, S., Capelli, R., Muccini, M., Ziessel, R. *J. Am. Chem. Soc.*, **2009**, *131*, 18177-18185.

(17) Lee, Y. O., Pradhana, T., No, K., Kim, J. S. *Tetrahedron*, **2012**, *68*, 1704-1711.

(18) Kim, H. M., Lee, Y. O., Lim, C. S., Kim, J. S., Cho, B. R. *J. Org. Chem.*, **2008**, *73*, 5127-5130.

(19) Sato, T., Uejima, M., Tanaka, K., Kaji, H., Adachi, C. *J. Mater. Chem. C*, **2015**, *3*, 870-878.

(20) Hu, J.-Y., Era, M., Elsegood, M. R. J., Yamato, T. *Eur. J. Org. Chem.*, **2010**, 72-79.

(21) Hu, J.-Y., Ni, X.-L., Feng, X., Era, M., Elsegood, M. R. J., Teat, S. J., Yamato, T. *Org. Biomol. Chem.*, **2012**, *10*, 2255-2262.

(22) Feng, X., Hu, J.-Y., Yi, L., Seto, N., Tao, Z., Redshaw, C., Elsegood, M. R. J., Yamato, T. *Chem. Asian J.*, **2012**, *7*, 2854-2863.

(23) Pope, M., Swenberg, C. E., Electronic Processes in Organic Crystals and Polymers, Oxford University Press: Oxford, **1999**, pp 48-53.

(24) Feng, X., Du, H., Chen, K., Xiao, X., Luo, S.-X., Xue, S.-F., Zhang, Y.-Q., Zhu, Q.-J., Tao, Z., Zhang, X.-Y., Wei, G. *Cryst Growth Des.*, **2010**, *10*, 2901-2907.

(25) Wang, C.-G., Chen, S.-Y., Wang, K., Zhao, S.-S., Zhang, J.-Y., Wang, Y. *J. Phys. Chem. C.*, **2012**, *116*, 17796−17806.

(26) Karmakar, S., Maity, D., Mardanya, S., Baitalik S. *J Phys Chem. A*, **2014**, *118*, 9397- 9410.

(27) (*a*) Sakuda, E., Ando, Y., Ito, A., Kitamura, N. *J. Phys. Chem. A*, **2010**, *114*, 9144-9150; (*b*) Ito, A., Kawanishi, K., Sakuda, E., Kitamura, N. *Chem. Eur. J.*, **2014**, *20*, 3940-3953.

(28) (*a*) Han, F., Chi, L., Wu, W., Liang, X., Fu, M., Zhao, J. *J. Photochem. Photobio. A: Chem.*, **2008**, *196*, 10-23; (*b*) Zhao, G.-J., Liu, J.-Y., Zhou, L.-C., Han, K.-L. *J. Phys. Chem. B*, **2007**, *111*, 8940-8945.

(29) Sciano, J. C. Handbook of Organic Photochemistry; CRC Press: Boca Raton, FL, **1989**.

(30) (a) Duong, H. M., Bendikov, M., Steiger, D., Zhang, Q., Sonmez, G., Yamada, J., Wudl, F. *Org. Lett.*, **2003**, *5*, 4433-4436; (b) Mardanya, S. Karmakar, S.; Das, S., Baitalik, S. *Sens Actuators B Chem.*, **2015**, *206*, 701-713.

(31) Crosby, G. A., Demas, J. N. *J. Phys. Chem.*, **1971**, *75*, 991-1024.

(32) SAINT, SMART and APEX 2 (**2000** & **2008**) software for CCD diffractometers. Bruker AXS Inc., Madison, USA.

(33) Programs CrysAlis-CCD and -RED, Oxford Diffraction Ltd., Abingdon, UK (**2013**).
(34) Palatinus, L., and Chapuis, G., *J. Appl. Cryst.* **2007**, *40*, 786-790.
(35) Sheldrick, G.M. *Acta Crystallogr*. **2008**, *A64*, 112-122